

Transferable E(3) equivariant parameterization for Hamiltonian of molecules and solids

Yang Zhong^{1,2}, Hongyu Yu^{1,2}, Mao Su^{1,2}, Xingao Gong^{1,2}, Hongjun Xiang^{1,2*}

¹Key Laboratory of Computational Physical Sciences (Ministry of Education), Institute of Computational Physical Sciences, State Key Laboratory of Surface Physics, and Department of Physics, Fudan University, Shanghai, 200433, China

²Shanghai Qi Zhi Institute, Shanghai, 200030, China

*E-mail: hxjiang@fudan.edu.cn

Abstract

Machine learning, especially deep learning, can build a direct mapping from structure to properties with its huge parameter space, making it possible to perform high-throughput screening for the desired properties of materials. However, since the electronic Hamiltonian transforms non-trivially under rotation operations, it is challenging to accurately predict the electronic Hamiltonian while strictly satisfying this constraint. There is currently a lack of transferable machine learning models that can bypass the computationally demanding density functional theory (DFT) to obtain the ab initio Hamiltonian of molecules and materials by complete data-driven methods. In this work, we point out the necessity of explicitly considering the parity symmetry of the electronic Hamiltonian in addition to rotational equivariance. We propose a parameterized Hamiltonian that strictly satisfies rotational equivariance and parity symmetry simultaneously, based on which we develop an E(3) equivariant neural network called HamNet to predict the ab initio tight-binding Hamiltonian of various molecules and solids. The tests show that this model has similar transferability to that of machine learning potentials and can be applied to a class of materials with different configurations using the same

set of trained network weights. The proposed framework provides a general transferable model for accelerating electronic structure calculations.

Introduction

Nowadays machine learning (ML) has a wide range of applications in molecular and materials science, including the direct prediction of various properties of materials¹⁻³, the construction of neural network (NN) potentials with quantum mechanical precision⁴⁻⁸, the high-throughput generation of molecular and crystal structures⁹⁻¹¹, and the construction of more precise exchange-correlation functionals^{12, 13}. However, the acquisition of the electronic structure of materials still relies almost exclusively on density functional theory (DFT) based calculations. Unfortunately, these methods are very time-consuming to get the Hamiltonian of the systems through self-consistent iterations and scale poorly with system size. Semi-empirical tight-binding (TB) approximations¹⁴, such as the Slater-Koster method¹⁵, can reduce a lot of computation compared to the ab initio DFT methods. However, this approach often directly uses the existing or manually fine-tuned TB parameters and thus cannot accurately reproduce the electronic structure of general systems. Machine learning methods have powerful fitting and inference capabilities, and can accurately fit the ab initio tight-binding Hamiltonian of the system by a fully data-driven method. Fitting the ab initio tight-binding Hamiltonian with ML can reconcile the accuracy with speed and can be used to accelerate large-scale electronic structure calculations in the same way as machine learning potentials in molecular dynamics (MD).

Hegde and Brown first used kernel ridge regression (KRR) to learn semi-empirical tight-binding Hamiltonian matrices¹⁶. They successfully fitted the Hamiltonian of the Cu system

containing only rotation invariant s orbitals and the diamond system consisting only of s and p orbitals. Similarly, Wang et al. designed a neural network model to obtain semi-empirical TB parameters by fitting the ab initio band structure¹⁷. An important feature of the Hamiltonian matrix is that its components transform equivariantly with the rotation of the coordinate system. However, neither of these approaches deals with the rotational equivariance of the Hamiltonian. Moreover, the two methods can only fit the empirical model Hamiltonian rather than the true ab initio tight-binding Hamiltonian generated by the self-consistent iteration of ab initio tight-binding methods based on numerical atomic orbitals such as OpenMX^{18, 19} and Siesta^{20, 21}.

Zhang et al.²² and Nigam et al.²³ proposed a method to predict the ab-initial TB Hamiltonian of small molecules and simple solid systems by constructing an equivariant kernel (kernel) in Gaussian Process Regression (GPR) to parameterize the Hamiltonian. Since GPR uses a fixed kernel and representation²⁴⁻²⁷, its training accuracy and multi-element generalization ability are usually lower than those of deep neural networks such as the message passing neural networks (MPNNs)²⁸⁻³³ when the number of training samples is sufficient. Therefore, developing graph neural networks (GNNs) capable of predicting the Hamiltonian of general periodic and aperiodic systems would be the best option.

However, traditional GNNs can only predict rotation-invariant scalars such as energy, band gap, etc. GNNs must encode the directional information of the system in an appropriate way to predict equivariant directional properties. In order to make the predicted Hamiltonian satisfy the rotational equivariance, Schütt et al. designed the SchNorb neural network architecture by embedding the direction information of the bonds into the message passing function³⁴. This network constructs the ab initio Hamiltonian of molecules from the directional edge features of

atom pairs. However, SchNorb needs to learn the rotational equivariance of the Hamiltonian through data augmentation, which greatly increases the amounts of training data and redundant parameters of the network. Unke et al proposed the PhisNet model³⁵, which realized the SE(3) equivariant parameterization of the Hamiltonian matrices with GNN based on SO(3) representations and achieved state-of-the-art accuracy on the Hamiltonian of small molecules such as water and ethanol. However, it should be noted that the PhisNet model is not the most universal representation of the Hamiltonian as it ignores the parity of the Hamiltonian, which may present serious problems when predicting periodical systems with infinite sizes. The limitations of SE(3) representation will be discussed in detail later.

Recently, Li et al. proposed a GNN model called DeepH to predict the ab initio Hamiltonian by constructing a local coordinate system in a crystal³⁶. DeepH successfully predicted the tight-binding Hamiltonian of some simple periodic systems such as graphene, carbon nanotubes, etc. Their original intention of introducing the local coordinate system is to solve the rotation equivariance problem of the Hamiltonian, but DeepH still embeds the local directional information of interacting atom pairs in the invariant message passing function, which will undoubtedly increase the number of redundant parameters of the network but may require less data augmentation than a fully invariant model without local coordinate systems. In addition, the hopping distance between two interacting atoms far exceeds the lengths of the general chemical bonds. Taking the smallest hydrogen atom as an example, the cutoff radius of the numerical atomic orbital of the hydrogen atom used by OpenMX is 6 Bohr, so the furthest hopping between any two atomic bases used by OpenMX in periodic systems can exceed at least 12 Bohr ($\sim 6.4 \text{ \AA}$), a distance that even exceeds the lattice parameters of some crystals. It

is difficult to describe such long hopping in a well-defined local coordinate system.

Currently, various reported machine learning models for fitting the Hamiltonian matrix can only be trained on a training set composed of materials with the same configuration and component, and be used to predict the Hamiltonian matrix of structures with small perturbations. Due to the lack of a general equivariant framework that can describe the ab initio tight-binding Hamiltonian of periodic and aperiodic systems, ML models of Hamiltonian matrices are still not sufficiently transferable and practical. In this work, we constructed a general parametrized Hamiltonian by decomposing each block of the Hamiltonian into a vector coupling of equivariant irreducible spherical tensors (ISTs) with correct parity. This parametrized Hamiltonian strictly satisfies the rotational equivariance and parity symmetry of the TB Hamiltonian of any periodic and aperiodic system. Based on this general parametrized Hamiltonian, we designed the E(3) equivariant HamNet model for predicting the ab initio TB Hamiltonian of molecules and solids. We successfully trained transferable HamNet models on the ab initio Hamiltonian datasets of QM9 molecules, carbon allotropes, Si allotropes, and SiO₂ isomers, respectively. The trained HamNet model can accurately predict the Hamiltonian matrices and energy band structures of the same type of structures of any size and configuration outside the training set. The HamNet model shows far more accuracy and transferability than the previously reported networks and is the first to be shown to have the prediction ability for structures with different configurations.

Results

E(3) equivariant parametrized Hamiltonian

The core of the electronic structure problem in DFT is to solve the Kohn-Sham equation for electrons in reciprocal space. If the Kohn-Sham Hamiltonian is expressed using numerical atomic orbitals centered on each atom (such as those defined in the OpenMX and Siesta code packages), then the Kohn-Sham equation can be expressed as a generalized eigenvalue problem as follows:

$$\mathbf{H}^{(\vec{k})} \psi_{n\vec{k}} = \varepsilon_{n\vec{k}} \mathbf{S}^{(\vec{k})} \psi_{n\vec{k}} \quad (1)$$

where $\mathbf{H}_{n_l, m_i, n_j, l, m_j}^{(\vec{k})} = \sum_{n_c} e^{i\vec{k} \cdot \vec{R}_{n_c}} \mathbf{H}_{n_l, m_i, n_j, l, m_j}^{(\vec{R}_{n_c})}$ and $\mathbf{S}_{n_l, m_i, n_j, l, m_j}^{(\vec{k})} = \sum_{n_c} e^{i\vec{k} \cdot \vec{R}_{n_c}} \mathbf{S}_{n_l, m_i, n_j, l, m_j}^{(\vec{R}_{n_c})}$ are the Kohn-Sham

Hamiltonian and overlap matrices at the point \vec{k} in the reciprocal space. $\mathbf{H}_{n_l, m_i, n_j, l, m_j}^{(\vec{k})}$ and

$\mathbf{S}_{n_l, m_i, n_j, l, m_j}^{(\vec{k})}$ are obtained by Fourier transform of real-space TB Hamiltonian matrix

$\mathbf{H}_{n_l, m_i, n_j, l, m_j}^{(\vec{R}_{n_c})} = \langle \phi_{n_l, m_i}(\vec{r} - \vec{\tau}_i) | \hat{H} | \phi_{n_j, l, m_j}(\vec{r} - \vec{\tau}_j - \vec{R}_{n_c}) \rangle$ and overlap matrix

$\mathbf{S}_{n_l, m_i, n_j, l, m_j}^{(\vec{R}_{n_c})} = \langle \phi_{n_l, m_i}(\vec{r} - \vec{\tau}_i) | \phi_{n_j, l, m_j}(\vec{r} - \vec{\tau}_j - \vec{R}_{n_c}) \rangle$ in the basis of atomic orbitals ϕ_{n_l, m_i} at the site

$\vec{\tau}_i$ and ϕ_{n_j, l, m_j} at the site $\vec{\tau}_j + \vec{R}_{n_c}$, where \vec{R}_{n_c} is the shift vector of periodic image cell.

Therefore, once we have obtained the Hamiltonian matrix and overlap matrix in real space, we can further solve the electronic structure in the whole reciprocal space.

Due to the spherical symmetry of the atomic potential, the atomic orbital base as its eigenfunction not only satisfies the rotational equivariance under the operation $Q \in SO(3)$ but also has a certain parity symmetry under the inversion operation $g \in \{E, I\}$. Under any rotatory inversion operation $gQ \in O(3)$, the TB Hamiltonian matrix element $\mathbf{H}_{n_l, m_i, n_j, l, m_j}$ in

real space becomes (we omit the notation \vec{R}_{n_c} for convenience in the following discussion):

$$\mathbf{H}'_{n_i l_i m_i, n_j l_j m_j} = \langle gQ\phi_{n_i l_i m_i} | \hat{H} | gQ\phi_{n_j l_j m_j} \rangle. \quad (2)$$

The irreducible representation of gQ is $\sigma_p(g) \otimes D(Q)$, where $D(Q)$ is the Wigner D matrix and $\sigma_p(g)$ is the scalar irreducible representation of the inversion operation, which is defined as follows

$$\sigma_p(g) = \begin{cases} 1, & g = E \\ p, & g = I \end{cases}. \quad (3)$$

Substitute the irreducible representation of gQ into Eq. (2), we can get

$$\mathbf{H}'_{n_i l_i m_i, n_j l_j m_j} = \sigma_{p_i p_j}(g) \sum_{\mu_i \mu_j} D_{\mu_i m_i}^{(l_i)}(\hat{R}) D_{\mu_j m_j}^{(l_j)}(\hat{R}) \mathbf{H}_{n_i l_i \mu_i, n_j l_j \mu_j}, \quad (4)$$

where $\sigma_{p_i p_j}(g) = \sigma_{p_i}(g) \sigma_{p_j}(g)$. We further write the right-hand side of Eq. (4) in the form of matrix-vector multiplication:

$$\mathbf{H}'_{n_i l_i m_i, n_j l_j m_j} = \sigma_{p_i p_j}(g) \sum_{\mu_i \mu_j} \left[D^{l_i}(\hat{R}) \otimes D^{l_j}(\hat{R}) \right]_{\mu_i \mu_j, m_i m_j} \mathbf{H}_{n_i l_i \mu_i, n_j l_j \mu_j}. \quad (5)$$

It can be seen from the above equation that each sub-block $\mathbf{H}_{n_i l_i \mu_i, n_j l_j \mu_j} (|\mu_i| \leq l_i, |\mu_j| \leq l_j)$ of the tight-binding Hamiltonian based on atomic orbitals can be regarded as a spherical tensor $T_{\mu, p_i p_j}^{n_i l_i, n_j l_j} \equiv \mathbf{H}_{n_i l_i \mu_i, n_j l_j \mu_j}$ with the parity $p_i p_j$, which is rotational equivariant according to the generalized Wigner D matrix $D_{\mu m}^l(\hat{R}) = D_{\mu m}^{l_i}(\hat{R}) D_{\mu m}^{l_j}(\hat{R})$, where $\mathbf{l} = (l_i, l_j)$, $\boldsymbol{\mu} = (\mu_i, \mu_j)$, $\mathbf{m} = (m_i, m_j)$.

According to the angular momentum theory, $D^{l_i}(\hat{R}) \otimes D^{l_j}(\hat{R})$ is a reducible representation, which can be further decomposed into the direct sum of several irreducible Wigner D matrices:

$$D^{l_i} \otimes D^{l_j} = D^{|\mu_i - \mu_j|} \oplus D^{|\mu_i - \mu_j| + 1} \oplus \dots \oplus D^{l_i + l_j}. \quad (6)$$

Combining the parity of the Hamiltonian matrix block $(n_i l_i, n_j l_j)$, we can get

$$\sigma_{p_i p_j}(\mathbf{g}) D^{l_i}(\hat{R}) \otimes D^{l_j}(\hat{R}) = \sum_{L=|l_i-l_j|}^{l_i+l_j} \oplus \sigma_{p_i p_j}(\mathbf{g}) D^L(\hat{R}) \quad (7)$$

According to Eq. (7), $\mathbf{T}_{\mu, p_i p_j}^{n_i l_i, n_j l_j}$ is reducible and the coupled irreducible spherical tensor (IST)

$T_{L, p_i p_j, m}^{n_i l_i, n_j l_j}$ in each order $L = |l_i - l_j|, \dots, l_i + l_j$ subspace can be obtained by the vector coupling

of $\mathbf{T}_{\mu, p_i p_j}^{n_i l_i, n_j l_j}$:

$$T_{L, p_i p_j, m}^{n_i l_i, n_j l_j} = \sum_{\mu_i = -l_i}^{l_i} \sum_{\mu_j = -l_j}^{l_j} C_{m \mu_i \mu_j}^{L l_i l_j} \mathbf{T}_{\mu, p_i p_j}^{n_i l_i, n_j l_j}, \quad (8)$$

where $C_{m \mu_i \mu_j}^{L l_i l_j}$ is the vector coupling coefficient, namely the Clebsch-Gordan coefficient. Each

IST $T_{L, p_i p_j, m}^{n_i l_i, n_j l_j}$ has the parity symmetry of $p_i p_j$ and satisfies the rotational equivariance of

order L . By inverse linear transformation of Eq. (8), $\mathbf{T}_{\mu, p_i p_j}^{n_i l_i, n_j l_j}$ can be constructed from ISTs

$T_{L, p_i p_j, m}^{n_i l_i, n_j l_j}$:

$$\mathbf{T}_{\mu, p_i p_j}^{n_i l_i, n_j l_j} = \sum_{L=|l_i-l_j|}^{l_i+l_j} \sum_{m=-L}^L C_{\mu, \mu_j m}^{L l_i l_j} T_{L, p_i p_j, m}^{n_i l_i, n_j l_j} \quad (9)$$

Therefore, as long as we find all ISTs corresponding to each block of the Hamiltonian matrix,

we can construct the entire Hamiltonian matrix in a block-wise manner through Eq. (9). We

construct two O(3) equivariant vectors $\mathbf{\Omega}_i^{on}$ and $\mathbf{\Omega}_{ij}^{off}$ by direct summation of all the ISTs

required by the on-site ($i = j$) Hamiltonian and the off-site ($i \neq j$) Hamiltonian respectively:

$$\mathbf{\Omega}_i^{on} = \sum_{n_i l_i} \sum_{n_i' l_i'} \sum_{L=|l_i-l_i'|}^{l_i+l_i'} \oplus \left[T_{L, p_i p_i, m}^{n_i l_i, n_i' l_i'} \right]_{-L \leq m \leq L} \quad (10)$$

$$\mathbf{\Omega}_{ij}^{off} = \sum_{n_i l_i} \sum_{n_j l_j} \sum_{L=|l_i-l_j|}^{l_i+l_j} \oplus \left[T_{L, p_i p_j, m}^{n_i l_i, n_j l_j} \right]_{-L \leq m \leq L} \quad (11)$$

The prediction of the Hamiltonian is transformed into the prediction of $\mathbf{\Omega}_i^{on}$ and $\mathbf{\Omega}_{ij}^{off}$, which

can be obtained by mapping from the equivariant features of the nodes and the pair interactions, respectively. The final parameterized Hamiltonian can be expressed as:

$$\tilde{H}_{n_i l_i m_i, n_j l_j m_j} = \begin{cases} \tilde{H}_{n_i l_i m_i, n_i' l_i' m_i'}^{on} = \sum_{L=|l_i-l_i'|}^{l_i+l_i'} \sum_{m=-L}^L C_{m_i, m_i', m}^{l_i, l_i', L} T_{L, p_i, p_i', m}^{n_i l_i, n_i' l_i'} & i = j \\ \tilde{H}_{n_i l_i m_i, n_j l_j m_j}^{off} = \sum_{L=|l_i-l_j|}^{l_i+l_j} \sum_{m=-L}^L C_{m_i, m_j, m}^{l_i, l_j, L} T_{L, p_i, p_j, m}^{n_i l_i, n_j l_j} & i \neq j \end{cases} \quad (12)$$

The above formula is O(3) equivariant. Since GNN naturally has translational symmetry, the parameterized Hamiltonian represented by Ω_i^{on} and Ω_{ij}^{off} obtained from GNN has E(3) equivariance.

Network Implementation

As can be seen from the above discussion, the Hamiltonian matrix block satisfies the rotation equivariance and has a definite parity under the inversion operation, so we designed E(3) equivariant HamNet deep neural network based on MPNN to fit ab initio TB Hamiltonian. This framework directly captures the electronic structure without expensive self-consistent iterations by constructing local equivariant representations of each atomic orbital, which is similar to the idea of the local density approximation of DFT. The network architecture of HamNet is shown in Fig. 1(a). HamNet can achieve a direct mapping from atomic species $\{Z_i\}$ and positions $\{\vec{r}_i\}$ to ab initio TB Hamiltonians. HamNet first encodes elements, inter-atomic distances, and relative directions as initial graph embeddings.

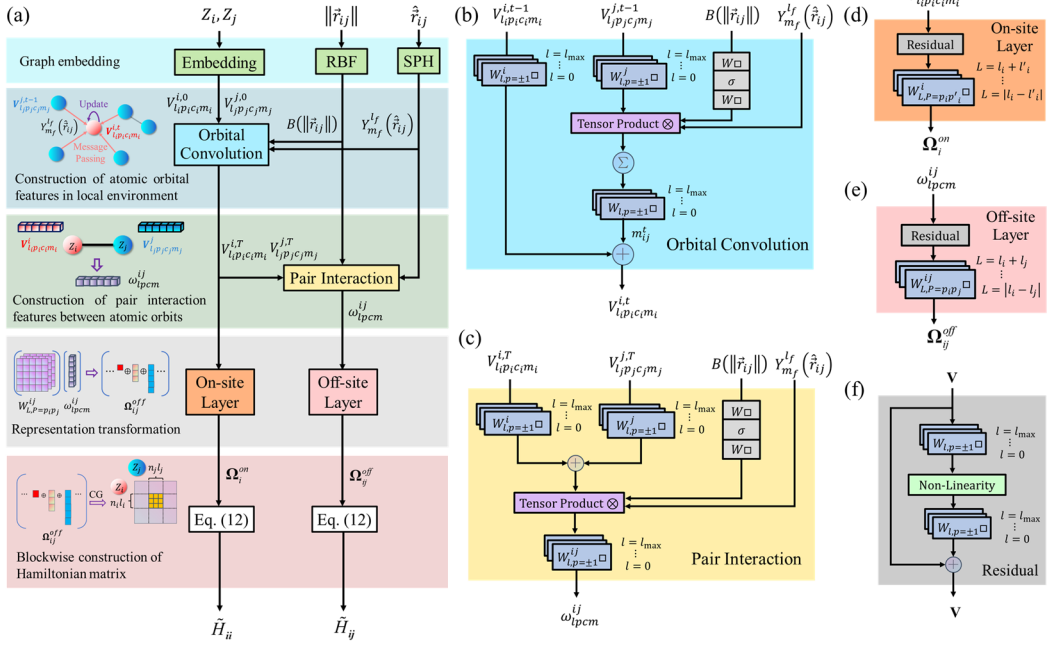


Fig. 1. HamNet architecture and the illustration of its subnetworks. (a) The overall architecture of HamNet. This neural network architecture predicts the Hamiltonian matrix through 5 steps. The prediction starts from the initial graph embedding of the species, interatomic distances, and interatomic directions of molecules and crystals. The atomic orbital features with angular momentum l in the local environment are included in the l -order components of the E(3) equivariant atom features and are refined through T orbital convolution blocks. In the third step, pair interaction features $\omega_{l,p,c,m}^{ij}$ of atomic orbitals are constructed by pair interaction blocks.

In the fourth step, the IST representations of on-site and off-site Hamiltonian matrices are constructed by passing the features of atomic orbitals and pair interactions through the on-site layer and off-site layer, respectively. The final step is to construct the on-site and off-site Hamiltonian matrices block-by-block via the parameterized Hamiltonian given by Eq. (12). (b) Orbital convolution block. The equivariant atomic features that include the features of atomic orbitals of each angular momentum l are refined by the equivariant message passing and update functions. (c) Pair interaction block. This block is used to construct the interaction features between the orbitals of two adjacent atoms. The orbital features of the central atom i and the neighboring atom j are first coupled and then scaled by tensor products according to the orientation and distance between the atoms. (d) On-site layer. The equivariant features of atoms are transformed into ISTs of on-site blocks Ω_i^{on} by the on-site layer. (e) Off-site layer. The pair interaction features between atomic orbitals are transformed into ISTs of the off-site block by the off-site layer. (f) Residual block. The residual block is used in the on-site layer and off-site layer to perform a nonlinear equivariant transformation of input features.

The distance between atom i and its neighboring atom j within the cutoff radius r_c is expanded using the Bessel basis function:

$$B(\|\vec{r}_{ij}\|) = \sqrt{\frac{2}{r_c}} \frac{\sin(n\pi \|\vec{r}_{ij}\|/r_c)}{\|\vec{r}_{ij}\|} f_c(\|\vec{r}_{ij}\|), \quad (13)$$

where f_c is the cosine cutoff function, which guarantees physical continuity as atoms enter and exit the cutoff sphere. The directional information between atom i and atom j is embedded in a set of real spherical harmonics $\{Y_{m_f}^{l_f}(\hat{r}_{ij})\}$, which is used to construct the rotation-equivariant filter³⁷ in the equivariant message passing.

The atomic feature $\mathbf{V} = V_{l_0 p_0} \oplus V_{l_1 p_1} \oplus \dots \oplus V_{l_{\max} p_{\max}}$ in HamNet is represented by a direct sum of different O(3) representations up to l_{\max} order, and each order feature can characterize the atomic orbit with different angular quantum numbers. Such features are transformed by the direct sum of the Wigner D matrix, i.e. by the block diagonal matrix $\mathbf{D} = D_{l_0} \oplus D_{l_1} \oplus \dots \oplus D_{l_{\max}}$. $V_{l_i, p_i, c_i, m_i}^{i, t}$ denotes the equivariant features of atom i in the orbital convolution layer t , where $l_i \leq l_{\max}$ is the order of the O(3) irreducible representation, $p_i \in \{1, -1\}$ denotes the parity of the equivariant components of the order l_i , $-l_i \leq m_i \leq l_i$ is the index of each projection of the equivariant representation, c_i is the channel index. We use T orbital convolution layers to construct the equivariant features of the atomic orbits in the local environment. Each orbital convolution layer performs a tensor product of the equivariant features of the neighbor atomic orbits and the spherical harmonic embeddings of the edge directions via Eq. (14), and the invariant scalar features of the interatomic distance are used to scale the equivariant output of each angular momentum. The message $m_{l_i, p_i, c_i, m_i}^{ij, t}$ output by Eq. (14) is composed of contributions with parity $p_i = p_j p_f$ to satisfy parity symmetry. Eq. (15) is the update function

of orbital equivariant features.

$$m_{l_i, p_i, c_i, m_i}^{ij, t} = \sum_{m_f = -l_f}^{l_f} \sum_{m_j = -l_j}^{l_j} C_{m_i, m_f, m_j}^{l_i, l_f, l_j} \text{MLP} \left[B(r_{ij}) \right]_{l_f, p_f, l_j, p_j}^{l_i, p_i, c_i} Y_{m_f}^{l_f} \left(\hat{r}_{ij} \right) V_{l_j, p_j, c_j, m_j}^{j, t-1} \quad (14)$$

$$V_{l_i, p_i, c_i, m_i}^{i, t} = V_{l_i, p_i, c_i, m_i}^{i, t-1} + \sum_{j \in N(i)} m_{l_i, p_i, c_i, m_i}^{ij, t} \quad (15)$$

The pair interaction layer adjusts the pair interaction features (used to construct off-site Hamiltonian) based on the features of the atomic orbitals of two interacting atoms as well as the direction and strength of their interactions.

$$\omega_{l', p', c, m}^{ij} = \sum_{m_f = -l_f}^{l_f} \sum_{m' = -l'}^{l'} C_{m', m_f, m}^{l', l_f, l} \text{MLP} \left[B(r_{ij}) \right]_{l_f, p_f, l', p'}^{l', p, c} Y_{m_f}^{l_f} \left(\hat{r}_{ij} \right) V_{l', p', c, m'}^{ij} \quad (16)$$

$$V_{l', p', c, m'}^{ij} = \sum_{c'} W_{l', p', c, c'}^i V_{l', p', c', m'}^{i, T} + \sum_{c'} W_{l', p', c, c'}^j V_{l', p', c', m'}^{j, T} \quad (17)$$

$V_{l', p', c, m'}^{ij}$ is the mixed feature vector of the equivariant linearly transformed features of $V_{l_i, p_i, c_i, m_i}^{i, T}$ and $V_{l_j, p_j, c_j, m_j}^{j, T}$. The on-site layer and off-site layer are used to convert the node features $V_{l_i, p_i, c_i, m_i}^{i, T}$ and pair interaction features $\omega_{l', p', c, m}^{ij}$ into the direct sums Ω_i^{on} and Ω_{ij}^{off} of the ISTs required to construct on-site and off-site Hamiltonian blocks, respectively. We add shortcut connections in the on-site layer and off-site layer and also use a multilayer perceptron (MLP) that scales the modulus of the irreducible representations of each order nonlinearly to increase the nonlinear fitting ability of the network. In the last step, the network uses each IST in Ω_i^{on} and Ω_{ij}^{off} to construct the on-site and off-site Hamiltonian blocks through Eq. (12). The predicted Hermitian Hamiltonian is obtained by the following symmetrization:

$$H_{n_i l_i m_i, n_j l_j m_j} = \begin{cases} H_{n_i l_i m_i, n_i l_i m_i}^{on} = \left(\tilde{H}_{n_i l_i m_i, n_i l_i m_i}^{on} + \tilde{H}_{n_i l_i m_i, n_i l_i m_i}^{on} \right) / 2 & i = j \\ H_{n_i l_i m_i, n_j l_j m_j}^{off} = \left(\tilde{H}_{n_i l_i m_i, n_j l_j m_j}^{off} + \tilde{H}_{n_j l_j m_j, n_i l_i m_i}^{off} \right) / 2 & i \neq j \end{cases} \quad (18)$$

Limitations of $SO(3)$ equivariant parametrized Hamiltonian

According to the previous symmetry analysis, each subblock of the TB Hamiltonian matrix not only satisfies the $SO(3)$ rotation equivariance but also has a certain parity. A parameterized Hamiltonian that only takes into account $SO(3)$ rotational equivariance without explicitly considering parity symmetry is not general. PhiSNet is an equivariant network that has achieved state-of-the-art accuracy in predicting the Hamiltonian matrix of small molecules. However, since the parameterized Hamiltonian used by PhiSNet is constructed from the $SO(3)$ irreducible representations, PhiSNet does not explicitly consider the parity of the Hamiltonian matrix. As a result, the parameterized Hamiltonian matrix constructed by PhiSNet cannot correctly fit the Hamiltonian matrix of some complex systems such as periodic solids.

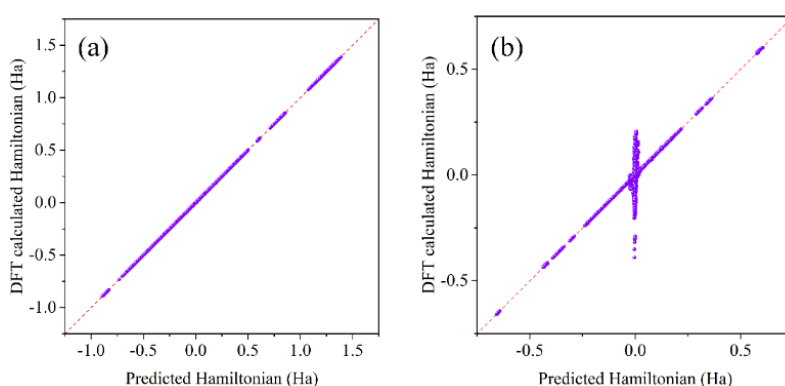


Fig. 2. Prediction results of PhiSNet for small molecules and periodic solids. (a) Comparison of the PhiSNet predicted Hamiltonian matrix elements and the OpenMX calculated Hamiltonian matrix elements on the test dataset of H₂O molecules. (b) Comparison of the PhiSNet predicted Hamiltonian matrix elements and the OpenMX calculated Hamiltonian matrix elements on the test dataset of graphene crystals.

We used the OpenMX calculated Hamiltonian matrices of 500 H₂O molecules (the molecular structure of H₂O comes from the training data of SchNorb³⁴) as the training, validation, and test sets of PhiSNet, respectively. Fig. 2(a) shows the scatter plot of the PhiSNet predicted Hamiltonian versus the DFT calculated Hamiltonian on the test dataset of H₂O molecules. All

scatter points are almost on the diagonal line. The mean absolute error (MAE) of PhiSNet on the test set of the water molecules is 1.99×10^{-5} Ha. We used the OpenMX calculated Hamiltonian of 225, 45, and 45 graphene structures as the training, validation, and test sets of PhiSNet, respectively. This dataset comes from the graphene dataset used by DeepH³⁸. Fig. 2(b) shows the scatter plot of the PhiSNet predicted Hamiltonian versus the DFT calculated Hamiltonian on the test dataset of graphene structures. It can be seen from Fig. 2(b) that some of the Hamiltonian matrix elements predicted by PhiSNet are incorrect and are always approximately zero, thus a vertical band appears at the zero point of Fig. 2(b).

Since the number of neighbors of each atom in a small molecule is at most the total number of atoms $- 1$, the number of hopping terms for small molecules to be fitted is small. The successful prediction of PhiSNet on the Hamiltonian of small molecules shows that it can adjust the network weights by training to make its output parameterized Hamiltonian have a pseudo parity, but this cannot ensure the strict parity symmetry of the Hamiltonian matrix intrinsically. In periodic crystal structures, the number of Hamiltonian matrices between each atom and its surrounding neighbors is much greater than that in small molecules. In this case, it is difficult for PhiSNet to satisfy the parity constraints of all Hamiltonian matrices, causing PhiSNet to fail in periodic solids. This test shows that the parameterized Hamiltonian matrices that only satisfy SO(3) equivariance are not universal, and it is necessary to explicitly consider parity symmetry for equivariant prediction of the Hamiltonian of materials, especially solids.

DeepH also does not explicitly consider the parity of Hamiltonian matrices. DeepH embeds the local cartesian information of each atomic pair in a non-equivariant way in the message passing function, so DeepH learns the parity symmetry by data augmentation and does not fail

in training and predicting the Hamiltonian of periodic solids.

Tests and applications

To test the accuracy and transferability of HamNet on periodic and aperiodic systems, we trained and tested HamNet on the Hamiltonian matrices for different configurations of QM9 molecules, carbon allotroths, Si allotroths, and SiO₂ isomers. Previously reported models such as SchNorb, PhiSNet and DeepH are trained and tested on only one configuration each time, and predicting the Hamiltonian matrix of a different configuration requires training these models on a new training set that consists of the perturbed structures of that configuration. Since HamNet is based on the universal parameterized Hamiltonian proposed in this work, our model can be trained and used on structures with the same atomic species but different configurations in the same way as ML force field models.

QM9 dataset.

The QM9 dataset^{39,40} contains 134k stable small organic molecules made up of CHONF. These small organic molecules are important candidates for drug discovery. The development of general ML models for rapid screening of the electronic structure properties of drug molecules is beneficial for understanding the mechanisms of drugs and shortening the cycle of drug development. We obtained the real-space ab initio TB Hamiltonian matrices calculated by OpenMX for 10,000 randomly selected molecules from the QM9 dataset. We used the Hamiltonian matrices of 8000 molecules as the training set, the Hamiltonian of 1000 molecules as the validation set, and the Hamiltonian of the remaining 1000 molecules as the test set. The MAE of the Hamiltonian matrix element predicted by the trained HamNet model on the test set

is only 1.49 meV. Fig. 3(a) shows the scatter plot of the HamNet predicted Hamiltonian matrix element versus the DFT calculated Hamiltonian matrix element on the test dataset, Fig 3(b) is the comparison of the HamNet predicted energy levels with the OpenMX calculated energy levels for 4 randomly selected molecules in the test set. As can be seen from Fig. 3, HamNet accurately predicted the Hamiltonian matrix element and energy levels of never encountered molecular structures outside the training set, showing excellent transferability. The HamNet model can build a general electronic structure model for small organic molecules such as drug molecules for high-throughput calculation of the electronic structures.

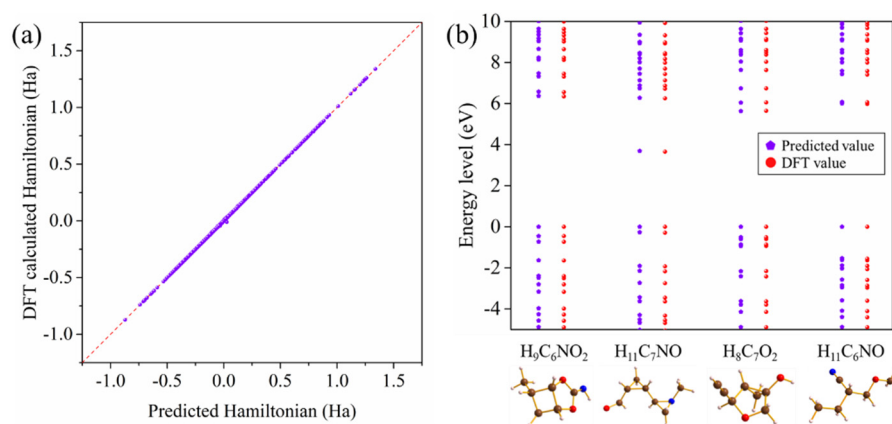


Fig. 3. Application of HamNet on molecules in the QM9 dataset. (a) Comparison of the HamNet predicted Hamiltonian matrix elements with the OpenMX calculated Hamiltonian matrix elements on the QM9 test set. (b) Comparison of predicted and calculated energy levels for 4 molecules randomly selected from the QM9 test set.

Carbon allotropes.

We collected 426 structures with less than 60 atoms in the primitive cell from Samara Carbon Allotrope Database (SACADA)⁴¹ and performed DFT calculations using OpenMX to obtain the ab initio Hamiltonian matrices for these structures. We divide these Hamiltonian data into the training set, validation set, and test set according to the ratio of 80%, 10%, and 10%. The MAE of the Hamiltonian matrix element predicted by HamNet on the test dataset is only 1.84

meV, which is even lower than the error (2.0 meV) of DeepH on the OpenMX calculated Hamiltonian dataset of only the graphene structures. HamNet was trained on the same graphene dataset used by DeepH and reached an MAE of only 0.49 meV on the test dataset. Most importantly, our HamNet model trained on the SACADA dataset is transferable and can fit the Hamiltonian of carbon allotropes of arbitrary sizes and configurations outside the training set.

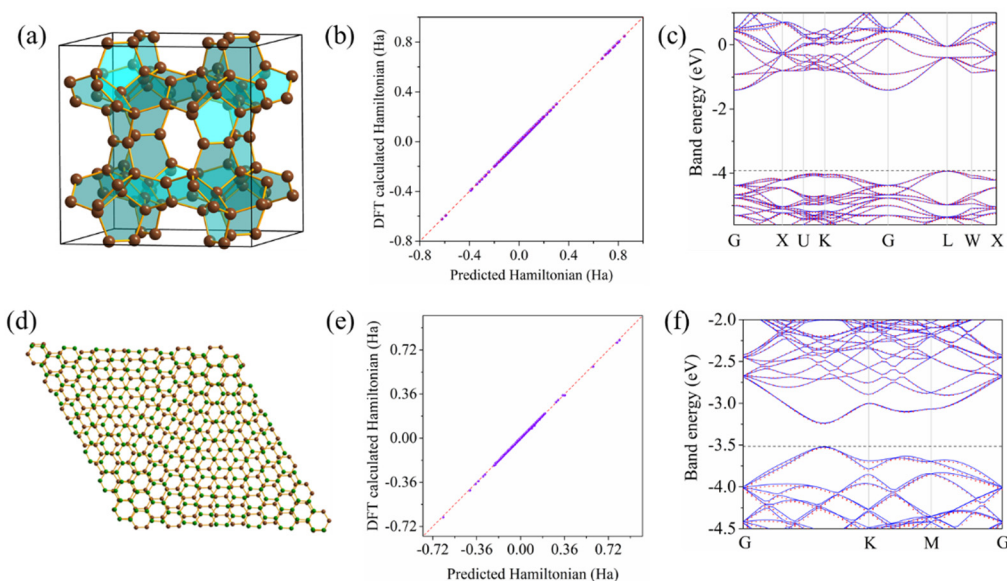


Fig. 4. Tests of HamNet on pentadiamond and twisted bilayer graphene (TBG). (a) Crystal structure of pentadiamond. (b) Comparison of the HamNet predicted Hamiltonian matrix elements and the DFT calculated Hamiltonian matrix elements of pentadiamond. (c) Comparison of HamNet predicted energy bands (solid line) and DFT calculated energy bands (dashed line) of pentadiamond. (d) Crystal structure of TBG with a twist angle of 5.09° . (e) Comparison of the HamNet predicted Hamiltonian matrix elements and the DFT calculated Hamiltonian matrix elements of TBG. (f) Comparison of the HamNet predicted energy bands (solid line) and the DFT calculated energy bands (dashed line) of TBG.

As shown in Fig 4, we used HamNet to predict the Hamiltonian as well as the band structure of pentadiamond⁴² and the twisted bilayer graphene (TBG) with a twist angle of 5.09° . Pentadiamond is a three-dimensional carbon foam constructed from carbon pentagons and contains 88 carbon atoms in a unit cell. The twist angle of the TBG structure (unrelaxed) used

for testing is about 5.09° , with a layer spacing of 3.5 Å and 508 carbon atoms in the unit cell. The MAE of the Hamiltonian matrix elements predicted by HamNet on the pentadiamond and the TBG is only 2.28 meV and 3.45 meV respectively. The energy bands calculated by the predicted Hamiltonian matrices are in high coincidence with those calculated by DFT. Note that DeepH has to be trained on untwisted bilayer graphene before predicting the TB Hamiltonian of TBG structures with the same layer spacing. The HamNet model trained on the SACADA carbon allotrope dataset is a universal model that can fit the Hamiltonian of any carbon allotrope structures. HamNet does not need to be trained on the training set built for the specific structure to be predicted, so the HamNet model is more practical and is similar to the usage of neural network potential used in molecular dynamics.

Silicon allotrope structure

There are a total of 39 Si allotropes in the Materials Project⁴³, from which we only collected 30 Si allotropes with less than 60 atoms per unit cell and calculated their ab initio TB Hamiltonian matrices with OpenMX. The Hamiltonian matrices of 24 randomly selected structures were used as the training set, the Hamiltonian matrices of 3 randomly selected structures were used as the verification set, and the Hamiltonian matrices of the remaining 3 structures were used as the test set. Although the Hamiltonian matrices of only 24 structures were used to train HamNet, the MAE of the HamNet model is only 1.79 meV and 2.60 meV on the validation set and test set, respectively. The fluctuation of the MAEs on the validation set and test set is mainly attributed to the limited total number of samples and that only a small number of samples are allocated to the test set and validation set. Therefore, it can be estimated that the actual MAE of the trained HamNet model should be between 1.79 and 2.60 meV.

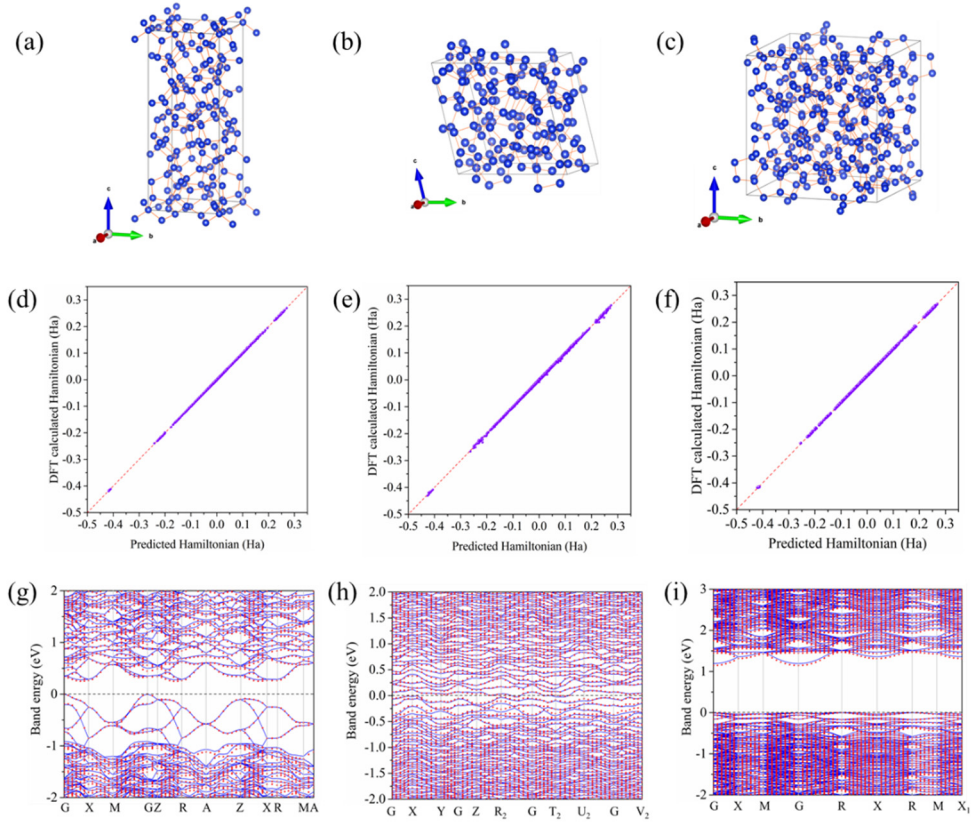


Fig. 5. Application of HamNet on three Si allotrope structures. (a-c) Crystal structures of mp-1204046, mp-1244971, and mp-1201492. (d-f) Comparison of the HamNet predicted Hamiltonian matrix elements and DFT calculated Hamiltonian matrix elements of mp-1204046, mp-1244971, and mp-1201492. (g-i) Comparison of the HamNet predicted energy bands (solid line) and the DFT calculated energy bands (dashed line) of mp-1204046, mp-1244971, and mp-1201492.

We selected three large Si allotropic structures (IDs on Materials Project are MP-1204046, MP-1244971, and MP-1201492 respectively) not included in the training set to test the accuracy and transferability of the trained HamNet model. The Si structure labeled MP-1204046 contains 106 atoms in the unit cell and belongs to the tetragonal system. Its structure is shown in Fig. 5(a). The MAE of the Hamiltonian matrix elements predicted by the HamNet model on mp-1204046 is only 1.75 meV, such a low error causes the predicted energy band to almost exactly coincide with the energy band calculated by DFT, as shown in Fig. 5(g). The structure of the Si allotrope labeled mp-1244971 is shown in Fig. 5(b). This structure is in an amorphous glassy state and quite different from the common four-coordinated Si allotrope. Each Si atom in this

structure is not always tetrahedral coordinated but forms an irregular polyhedron with 3–5 coordinating atoms, so the prediction difficulty for this Si structure is expected to be relatively high. However, HamNet still accurately predicted its Hamiltonian matrix and reached an MAE of 3.18 meV. The high prediction accuracy can be seen in the scatter plot of the predicted Hamiltonian matrix elements versus the DFT-computed Hamiltonian matrix elements shown in Fig. 5(e). The energy bands calculated from the predicted Hamiltonian are consistent with those calculated by DFT even at the energy levels very far from the Fermi level, as shown in Fig. 5(h).

The structure of the Si allotrope labeled mp-1201492 is shown in Fig. 5(c). This large structure contains 232 silicon atoms per unit cell and is built by the tetrahedra that share one or two vertices. The MAE of the Hamiltonian matrix elements predicted by the trained HamNet for this structure is only 1.63 meV. The closeness between the prediction and DFT calculation can be seen from the scatter plot of the predicted Hamiltonian matrix elements versus the DFT-computed Hamiltonian matrix elements shown in Fig. 5(f). It can be seen from Fig. 5(i) that the predicted energy bands coincide with the calculated energy bands in a large energy range around the band gap.

The HamNet model trained on only 24 small Si allotrope structures can already accurately predict the ab initio Hamiltonian matrix and energy bands of larger Si allotrope structures with different band gaps and configurations. The E(3) equivariant parameterized Hamiltonian proposed in this work strictly satisfies the SO(3) rotational equivariance and the parity symmetry of the Hamiltonian inherently, so it can achieve high accuracy and transferability without using huge training data to fit some unnecessary redundant parameters.

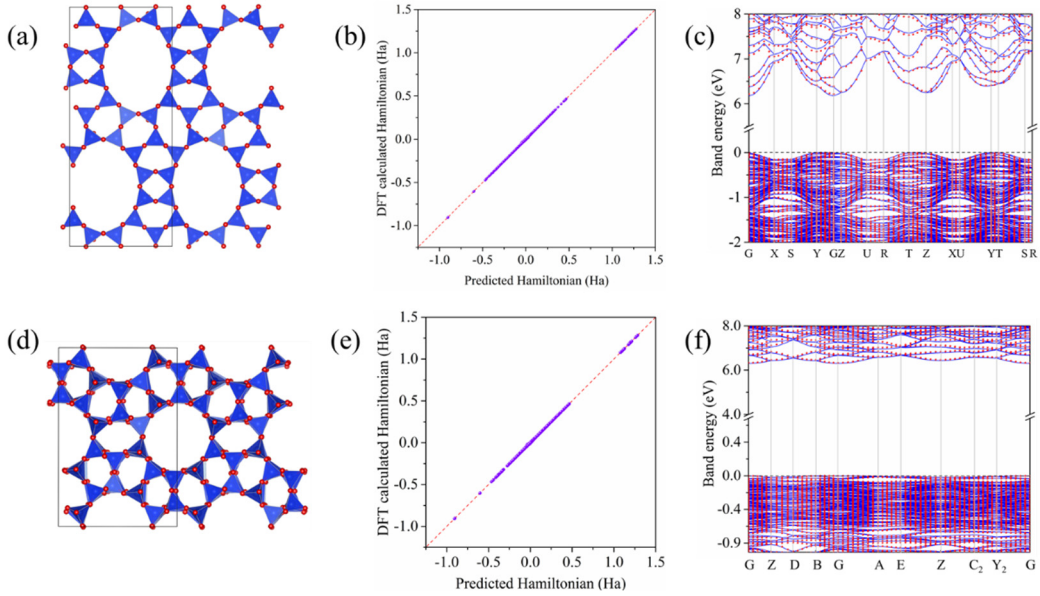


Fig. 6. The prediction results of HamNet for two SiO₂ structures. (a) Crystal structure of mp-667371. (b) Comparison of the predicted Hamiltonian matrix elements and the DFT calculated Hamiltonian matrix elements of mp-667371. (c) Comparison of the predicted energy bands (solid line) and DFT calculated energy bands (dashed line) of mp-667371. (d) Crystal structure of mp-1200292. (e) Comparison of the predicted Hamiltonian matrix elements and the DFT calculated Hamiltonian matrix elements of mp-1200292. (f) Comparison of the predicted energy bands (solid line) and DFT calculated energy bands (dashed line) of mp-1200292.

The isomers of Silicon dioxide.

Silicon dioxide is a binary compound with abundant isomeric structures. Building a transferable ML Hamiltonian model for the isomers of SiO₂ is a good test for the universality of our proposed parameterized Hamiltonian. We selected 187 SiO₂ structures with less than 60 atoms per cell from Materials Project and calculated their ab initio TB Hamiltonians using OpenMX. We divided all the calculated Hamiltonian matrices into the training set, validation set, and test set in a ratio of 0.8:0.1:0.1. The MAE of the Hamiltonian matrix elements predicted by the trained HamNet model on the test set is 3.75 meV.

The trained HamNet model was used to predict the ab initio Hamiltonian for two SiO₂ structures labeled mp-667371 and mp-1200292. They are characterized by the complex porous structures built by SiO₄ tetrahedra, as shown in Fig 6(a) and (d). mp-667371 has 168 atoms in

the primitive cell and belongs to the orthorhombic crystal system. mp-1200292 has 288 atoms in the primitive cell and belongs to the monoclinic crystal system. The MAE of the Hamiltonian matrix elements predicted by HamNet for mp-667371 and mp-1200292 is 3.32 meV and 3.05 meV, respectively. The accuracy of the predicted Hamiltonian can be seen in Fig. 6(b) and (e). The comparisons of the predicted and calculated energy bands of mp-667371 and mp-1200292 are shown in Fig. 6(c) and (f), respectively. The band gaps of both materials exceed 6 eV, and the energy bands predicted by HamNet and calculated by DFT almost exactly coincide in the wide energy range around the band gap. The successful application of HamNet on SiO₂ isomers shows that it can be used to bypass the expensive DFT calculation to study the electronic structure of large amorphous SiO₂ glass.

Discussion

Machine learning potentials with quantum mechanical precision are now widely used to accelerate long-time molecular dynamics simulations of large systems. However, there is still a lack of a general model that can build a direct mapping from structure to electronic Hamiltonian to quickly calculate and screen the electronic properties of materials. The machine learning Hamiltonian models reported so far only realize the training and fitting for the Hamiltonian of the molecules or crystals with the same configuration, and their transferability is thus far from that of machine learning potentials and hinders the application of these models on the prediction of electronic Hamiltonian. These models are not universal for the SO(3) rotation equivariance or the parity symmetry of the Hamiltonian matrix predicted by these models is not strictly satisfied. In this work, we compared the influence on the prediction of Hamiltonian with and without parity symmetry and pointed out the necessity of explicitly

considering the parity of Hamiltonian in the prediction. We proposed an analytical E(3) equivariant parameterized Hamiltonian that explicitly takes into account rotation equivariance and parity symmetry. Based on this parameterized Hamiltonian, we develop a deep neural network called HamNet to fit the Hamiltonian of arbitrary molecules and solids. Previously reported models were trained and tested on the datasets of the molecular dynamics perturbed molecules and solids with just the same configuration. To demonstrate the universality and transferability of this parameterized Hamiltonian, we directly train our model on real unperturbed structures with different configurations to obtain a general model to predict the Hamiltonian matrix and energy bands of various complex structures in the test set. Our training and testing process for the network is similar to that for general machine learning potentials. Actual tests show that the accuracy and transferability of HamNet are significantly better than those of previously reported models. Our work provides a general framework for practical applications of the prediction of Hamiltonian.

Methods

Hamiltonian datasets. QM9 structure set is available from <http://quantum-machine.org/datasets/>, SACADA structure set is available from https://www.sacada.info/sacada_3D.php, and the structures of Si allotropes and SiO₂ isomers are downloaded from the Materials Project site. We performed DFT calculations on the structures in the above datasets to obtain TB Hamiltonian matrices via OpenMX, a software package for nano-scale material simulations based on norm-conserving pseudopotentials and pseudo-atomic localized basis functions. H6.0-*s2p1*, C6.0-*s2p2d1*, N6.0-*s2p2d1*, O6.0-*s2p2d1*, F6.0-*s2p2d1*, and Si7.0-*s2p2d1* pseudoatomic orbitals (PAOs) were used as the basis for the calculations. The truncation radius of the atomic orbits of H, C, N, O, and F is 6.0 Bohr, and

the truncation radius of the atomic orbits of Si is 7.0 Bohr. A single Γ point is used to calculate the Hamiltonian for the QM9 molecule dataset and TBG, and a $6 \times 6 \times 6$ Monkhorst-Pack k point grid is used for the SACADA, Si, and SiO_2 datasets.

Network and training details. The Pytorch⁴⁴, PyG⁴⁵, Pytorch Lightning⁴⁶, Nequip³², and e3nn⁴⁷ libraries are used to implement HamNet. All models used in this work have five orbital convolution layers, a Pair Interaction layer, an on-site layer, and an off-site layer. Each atom is encoded as a one-hot vector of length 60 according to the atomic number, and the edge distances between each atom and its neighbors are expanded by eight Bessel function bases. The spherical harmonic functions with a maximum degree $L_{\max}=4$ are used to embed the directions of the edges. The $O(3)$ representations used for the atom features and pair interaction features have N_{fea} channels with a maximum degree L_{\max} and parities $p = \pm 1$. The number of feature channels N_{fea} and the maximum degree L_{\max} for each dataset are listed in Table 1. A two-layer MLP with 64 neurons is used to map the invariant edge embeddings to the weights of each tensor product path in Eqs. (14) and (16). Shifted softplus³⁰ function is used as the activation function in the MLP.

To avoid overfitting, we include the error of the calculated energy bands as a regularization term in the loss function:

$$L = \|\tilde{\mathbf{H}} - \mathbf{H}\| + \frac{\lambda}{N_{\text{orb}} \times N_k} \sum_{k=1}^{N_k} \sum_{n=1}^{N_{\text{orb}}} \|\tilde{\varepsilon}_{nk} - \varepsilon_{nk}\|, \quad (19)$$

where the variables marked with a tilde refer to the corresponding predictions and λ denotes the loss weight of the band energy error. When the training of the network has not converged, the error of the predicted Hamiltonian is large, resulting in poor or even divergent prediction values of the energy bands. Adding the band loss value at the beginning of training may cause the total loss value to diverge. Therefore, we train the network in two steps. First, only the mean absolute error of Hamiltonians is used as the loss value to train the network until the network weights converge. The parameters were optimized with AdamW^{48, 49} optimizer using an initial

learning rate of 10^{-3} . Then the mean absolute error of each band calculated at N_k random points in the reciprocal space is added to the loss function and starts the training at an initial learning rate of 10^{-4} . When the accuracy of the model on the validation set is not improved after successive N_{patience} epochs, the learning rate will be reduced by a factor of 0.5. When the accuracy of the model on the validation set is not improved after successive N_{stop} epochs or the learning rate is lower than 10^{-6} , the training will be stopped and the model that has the best accuracy on the validation set will be used on the test set. The values of some key network and training parameters on each dataset are listed in Table 1. All models were trained on a single NVIDIA A100 GPU.

Table 1. The network and training parameters used for Hamnet on each dataset.

Dataset	N_{batch}	N_{fea}	L_{max}	$r_{\text{cut}}(a_0)$	N_k	N_{patience}	N_{stop}
QM9	5	64	4	15.0	1	10	30
SACADA	1	32	4	20.0	5	5	30
Si	1	32	4	20.0	5	5	30
SiO ₂	1	32	4	20.0	5	5	30

Data and Code availability

The data and code that support the results of this work will be available online after the manuscript is accepted.

References

1. Choudhary, K. et al. High-throughput density functional perturbation theory and machine learning predictions of infrared, piezoelectric, and dielectric responses. *Npj Comput. Mater.* **6**, 64 (2020).
2. Liu, Y. T., Zhou, Q. & Cui, G. L. Machine Learning Boosting the Development of Advanced Lithium Batteries. *Small Methods* **5**, 2100442 (2021).
3. Zhang, N. et al. Machine Learning in Screening High Performance Electrocatalysts for CO₂ Reduction. *Small Methods* **5**, 2100987 (2021).
4. Manzhos, S. & Carrington, T., Jr. Neural Network Potential Energy Surfaces for Small Molecules and Reactions. *Chem Rev* **121**, 10187-10217 (2021).
5. Chen, C. & Ong, S. P. A Universal Graph Deep Learning Interatomic Potential for the Periodic Table. *Preprint at* <https://ui.adsabs.harvard.edu/abs/2022arXiv220202450C>

- (2022).
6. Choudhary, K. et al. Unified Graph Neural Network Force-field for the Periodic Table. *Preprint at* <https://ui.adsabs.harvard.edu/abs/2022arXiv220905554C> (2022).
 7. Cheng, Z. et al. Building quantum mechanics quality force fields of proteins with the generalized energy-based fragmentation approach and machine learning. *Phys. Chem. Chem. Phys.* **24**, 1326-1337 (2022).
 8. Unke, O. T. et al. SpookyNet: Learning force fields with electronic degrees of freedom and nonlocal effects. *Nat. Commun.* **12**, (2021).
 9. Cheng, G. J., Gong, X. G. & Yin, W. J. Crystal structure prediction by combining graph network and optimization algorithm. *Nat. Commun.* **13**, (2022).
 10. Ganea, O.-E. et al. GeoMol: Torsional Geometric Generation of Molecular 3D Conformer Ensembles. *Preprint at* <https://ui.adsabs.harvard.edu/abs/2021arXiv210607802G> (2021).
 11. Xie, T., Fu, X., Ganea, O.-E., Barzilay, R. & Jaakkola, T. Crystal Diffusion Variational Autoencoder for Periodic Material Generation. *Preprint at* <https://ui.adsabs.harvard.edu/abs/2021arXiv211006197X> (2021).
 12. Kirkpatrick, J. et al. Pushing the frontiers of density functionals by solving the fractional electron problem. *Science* **374**, 1385–1389 (2021).
 13. Nagai, R., Akashi, R. & Sugino, O. Machine-learning-based exchange correlation functional with physical asymptotic constraints. *Phys. Rev. Res.* **4**, 013106 (2022).
 14. Goringe, C. M., Bowler, D. R. & Hernandez, E. Tight-binding modelling of materials. *Rep. Prog. Phys.* **60**, 1447-1512 (1997).
 15. Papaconstantopoulos, D. A. & Mehl, M. J. The Slater-Koster tight-binding method: a computationally efficient and accurate approach. *J. Phys.: Condens. Matter* **15**, R413-R440 (2003).
 16. Hegde, G. & Bowen, R. C. Machine-learned approximations to Density Functional Theory Hamiltonians. *Sci. Rep.* **7**, 42669 (2017).
 17. Wang, Z. F. et al. Machine learning method for tight-binding Hamiltonian parameterization from ab-initio band structure. *Npj Comput. Mater.* **7**, 11 (2021).
 18. Ozaki, T. Variationally optimized atomic orbitals for large-scale electronic structures. *Phys. Rev. B* **67**, 155108 (2003).
 19. Ozaki, T. & Kino, H. Numerical atomic basis orbitals from H to Kr. *Phys. Rev. B* **69**, 195113 (2004).
 20. Artacho, E. et al. The SIESTA method; developments and applicability. *J. Phys.: Condens. Matter* **20**, 064208 (2008).
 21. Garcia, A. et al. Siesta: Recent developments and applications. *J. Chem. Phys.* **152**, 204108 (2020).
 22. Zhang, L. et al. Equivariant analytical mapping of first principles Hamiltonians to accurate and transferable materials models. *Preprint at* <https://doi.org/10.48550/arXiv.2111.13736> (2021).
 23. Nigam, J., Willatt, M. J. & Ceriotti, M. Equivariant representations for molecular Hamiltonians and N-center atomic-scale properties. *J. Chem. Phys.* **156**, 014115 (2022).
 24. Unke, O. T. & Meuwly, M. A reactive, scalable, and transferable model for molecular energies from a neural network approach based on local information. *J. Chem. Phys.* **148**, 241708 (2018).

25. Christensen, A. S., Bratholm, L. A., Faber, F. A. & Anatole von Lilienfeld, O. FCHL revisited: Faster and more accurate quantum machine learning. *J. Chem. Phys.* **152**, 044107 (2020).
26. Faber, F. A., Christensen, A. S., Huang, B. & von Lilienfeld, O. A. Alchemical and structural distribution based representation for universal quantum machine learning. *J. Chem. Phys.* **148**, 241717 (2018).
27. Bartok, A. P., Kondor, R. & Csanyi, G. On representing chemical environments. *Phys. Rev. B* **87**, 184115 (2013).
28. Gilmer, J., Schoenholz, S. S., Riley, P. F., Vinyals, O. & Dahl, G. E. Neural Message Passing for Quantum Chemistry. in *Proc. the 34th Int. Conf. on Machine Learning*, **70**, 1263–1272 (2017).
29. Xie, T. & Grossman, J. C. Crystal Graph Convolutional Neural Networks for an Accurate and Interpretable Prediction of Material Properties. *Phys. Rev. Lett.* **120**, 145301 (2018).
30. Schutt, K. T., Sauceda, H. E., Kindermans, P. J., Tkatchenko, A. & Muller, K. R. SchNet - A deep learning architecture for molecules and materials. *J. Chem. Phys.* **148**, 241722 (2018).
31. Choudhary, K. & DeCost, B. Atomistic Line Graph Neural Network for improved materials property predictions. *Npj Comput. Mater.* **7**, 185 (2021).
32. Batzner, S. et al. E(3)-equivariant graph neural networks for data-efficient and accurate interatomic potentials. *Nat. Commun.* **13**, 2453 (2022).
33. Wang, Z. et al. Heterogeneous relational message passing networks for molecular dynamics simulations. *Npj Comput. Mater.* **8**, 53 (2022).
34. Schutt, K. T., Gastegger, M., Tkatchenko, A., Muller, K. R. & Maurer, R. J. Unifying machine learning and quantum chemistry with a deep neural network for molecular wavefunctions. *Nat. Commun.* **10**, 5024 (2019).
35. Unke, O. T. et al. SE(3)-equivariant prediction of molecular wavefunctions and electronic densities. *Preprint at* <https://ui.adsabs.harvard.edu/abs/2021arXiv210602347U> (2021).
36. Li, H. C., Collins, C., Tanha, M., Gordon, G. J. & Yaron, D. J. A Density Functional Tight Binding Layer for Deep Learning of Chemical Hamiltonians. *Journal of Chemical Theory and Computation* **14**, 5764-5776 (2018).
37. Thomas, N. et al. Tensor field networks: Rotation- and translation-equivariant neural networks for 3D point clouds. *Preprint at* <https://arxiv.org/abs/1802.08219v3> (2018).
38. Li, H. et al. Deep Neural Network Representation of Density Functional Theory Hamiltonian. *Preprint at* <https://doi.org/10.48550/arXiv.2104.03786> (2021).
39. Ruddigkeit, L., van Deursen, R., Blum, L. C. & Reymond, J. L. Enumeration of 166 Billion Organic Small Molecules in the Chemical Universe Database GDB-17. *J. Chem. Inf. Model.* **52**, 2864-2875 (2012).
40. Ramakrishnan, R., Dral, P. O., Rupp, M. & von Lilienfeld, O. A. Quantum chemistry structures and properties of 134 kilo molecules. *Sci. Data* **1**, 140022 (2014).
41. Hoffmann, R., Kabanov, A. A., Golov, A. A. & Proserpio, D. M. Homo Citans and Carbon Allotropes: For an Ethics of Citation. *Angew. Chem. Int. Edit.* **55**, 10962-10976 (2016).
42. Fujii, Y., Maruyama, M., Cuong, N. T. & Okada, S. Pentadiamond: A Hard Carbon Allotrope of a Pentagonal Network of $\{\mathrm{sp}\}^2$ and $\{\mathrm{sp}\}^3$ C Atoms. *Phys. Rev. Lett.* **125**, 016001 (2020).

43. Jain, A. et al. Commentary: The Materials Project: A materials genome approach to accelerating materials innovation. *APL Mater.* **1**, 011002 (2013).
44. Paszke, A., Gross, S., Massa, F., Lerer, A. & Chintala, S. PyTorch: An Imperative Style, High-Performance Deep Learning Library. *Preprint at* <https://arxiv.org/abs/1912.01703> (2019).
45. Fey, M. & Lenssen, J. E. Fast Graph Representation Learning with PyTorch Geometric. *Preprint at* <https://ui.adsabs.harvard.edu/abs/2019arXiv190302428F> (2019).
46. Pytorch Lightning website. <https://www.pytorchlightning.ai/>.
47. Geiger, M. et al. e3nn/e3nn: 2022-04-13 (0.5.0). <https://doi.org/10.5281/zenodo.6459381> (2022).
48. Loshchilov, I. & Hutter, F. Decoupled Weight Decay Regularization. *Preprint at* <https://doi.org/10.48550/arXiv.1711.05101> (2017).
49. Reddi, S. J., Kale, S. & Kumar, S. On the Convergence of Adam and Beyond. *Preprint at* <https://ui.adsabs.harvard.edu/abs/2019arXiv190409237R> (2019).